Phytochemistry 243 (2026) 114735

Contents lists available at ScienceDirect

Phytochemistry

journal homepage: www.elsevier.com/locate/phytochem

Phytochemical study of *Fissistigma fulgens* (Hook.f. & Thomson) Merr. leaves: Previously undescribed dihydrochalcone derivatives and their biological activities

Passakorn Teerapongpisan [a,b], Wuttichai Jaidee [c], Theanchai Wiwasuku [d,e], Sarot Cheenpracha [f], Natcha Injan [f], Somkiat Nokbin [g,h], Kittirat Saharat [i], Atthapan Morchang [j,k], Phateep Hankittichai [j,k], Rawiwan Charoensup [c,l], Raymond J. Andersen [m], Surat Laphookhieo [n,*]

[a] *Futuristic Science Research Center, School of Science, Walailak University, Nakhon Si Thammarat, 80160, Thailand*
[b] *Research Center for Theoretical Simulation and Applied Research in Bioscience and Sensing, Walailak University, Nakhon Si Thammarat, 80160, Thailand*
[c] *Medicinal Plant Innovation Center of Mae Fah, Luang University, Chiang Rai, 57100, Thailand*
[d] *School of Science, Walailak University, Nakhon Si Thammarat, 80161, Thailand*
[e] *Functional Materials and Nanotechnology Center of Excellence, Walailak University, Nakhon Si Thammarat, 80161, Thailand*
[f] *Division of Chemistry, School of Science, University of Phayao, Phayao, 56000, Thailand*
[g] *Laboratory for Computational and Applied Chemistry, Department of Chemistry, Faculty of Science, Kasetsart University, Bangkok, 10900, Thailand*
[h] *Center for Advanced Studies in Nanotechnology for Chemical, Food and Agricultural Industries, Kasetsart University Institute for Advanced Studies, Kasetsart University, Bangkok, 10900, Thailand*
[i] *School of Science, Mae Fah Luang University, Chiang Rai, 57100, Thailand*
[j] *School of Medicine, Mae Fah Luang University, Chiang Rai, 57100, Thailand*
[k] *Cancer and Immunology Research Unit (CIRU), Mae Fah Luang University, Chiang Rai, 57100, Thailand*
[l] *School of Integrative Medicine, Mae Fah Luang University, Chiang Rai, 57100, Thailand*
[m] *Departments of Chemistry and Earth, Ocean & Atmospheric Sciences, University of British Columbia, 2036 Main Mall, Vancouver, BC, V6T 1Z1, Canada*
[n] *Center of Chemical Innovation for Sustainability (CIS), Mae Fah Luang University, Chiang Rai, 57100, Thailand*

ARTICLE INFO

Keywords:
Fissistigma fulgens
Annonaceae
Dihydrochalcones
Cytotoxicity
Anti-DENV
Nitric oxide production inhibitory activity

ABSTRACT

The first phytochemical investigation of the leaves of *Fissistigma fulgens* (Hook.f. & Thomson) Merr. led to the isolation and identification of five previously undescribed dihydrochalcone derivatives, including two dimeric dihydrochalcones, fissisfulgenones A and B (**1** and **2**), and three monomeric dihydrochalcones, fissisfulgenones C–E (**3**–**5**), along with three known compounds. Their structures were elucidated by spectroscopic analysis. The dimeric structure of fissisfulgenone A (**1**) was confirmed by single-crystal X-ray diffraction analysis using Cu–Kα radiation. The pure enantiomers of the scalemic mixtures of **1**–**3** were successfully resolved using chiral-phase HPLC, and their absolute configurations were determined by comparing experimental and calculated ECD spectra. Fissisfulgenones A (**1**), C (**3**), and D (**4**) were evaluated for biological activities, including cytotoxicity against human breast adenocarcinoma (MDA-MB231), human lung carcinoma (A549), human hepatocellular carcinoma (Huh7), and human colorectal adenocarcinoma (SW480 and HT29), antiviral activity against dengue virus (DENV), and nitric oxide production inhibitory activity in LPS-stimulated RAW 264.7 macrophages. Among them, fissisfulgenone C (**3**) exhibited the highest cytotoxicity against SW480 and HT29 cells with IC_{50} values of 40.6 and 68.0 μM, respectively, whereas fissisfulgenone D (**4**) showed cytotoxicity against MDA-MB231, A549, and Huh7 cell lines with IC_{50} values of 48.7, 38.3, and 21.2 μM, respectively. Notably, fissisfulgenone A (**1**) significantly reduced virus production in DENV-infected Huh7 cells at a sub-toxic dose of 50.0 μM. Regarding anti-inflammatory activity, fissisfulgenone C (**3**) exhibited strong nitric oxide inhibition, markedly reducing LPS-induced levels with an IC_{50} value of 5.27 μM and preserving normal macrophage morphology. Fissisfulgenone A (**1**) also showed similar effects at lower, non-toxic concentrations.

* Corresponding author.
E-mail address: surat.lap@mfu.ac.th (S. Laphookhieo).

https://doi.org/10.1016/j.phytochem.2025.114735
Received 7 July 2025; Received in revised form 24 November 2025; Accepted 29 November 2025
Available online 2 December 2025

1. Introduction

Chalcone derivatives, a class of polyphenolic specialized metabolites with wide structural diversity, are biosynthesized via the phenylpropanoid pathway (Lam et al., 2021). These compounds are widely distributed among plant families, particularly the Annonaceae (Auranwiwat et al., 2018; Chen et al., 2021; Jaidee et al., 2019; Jin et al., 2023; Koudokpon et al., 2018; Lan et al., 2011; Ngoc et al., 2019; Salae et al., 2017; Wirasathien et al., 2006). Several genera within this family, including *Uvaria*, *Melodorum*, and *Fissistigma*, are recognized as rich sources of chalcone derivatives with diverse biological activities. Due to their promising pharmacological properties, chalcones have attracted attention for their antioxidant, anti-inflammatory, anticancer, and antiviral effects (Chen et al., 2021; Jaidee et al., 2019; Jin et al., 2023; Lan et al., 2011; Ngoc et al., 2019; Salae et al., 2017; Wirasathien et al., 2006).

Notably, dihydrochalcone derivatives from *Fissistigma* species have demonstrated broad-spectrum bioactivities. For instance, 4′,5′-dimethoxy-2′-hydroxy-3′,6′-quinodihydrochalcone, isolated from *F. oldhamii*, exhibited potent cytotoxicity against the HEPG2 liver cancer cell line (IC_{50} = 10.8 μM) (Chen et al., 2021). Another compound, 4,6-dimethoxy-2,5-quinodihydrochalcone from *F. latifolium*, demonstrated cytotoxicity against MDA-MB231 breast cancer cells (IC_{50} = 7.1 μM) (Lan et al., 2011). Similarly, adunctin E, derived from *F. cupreonitens*, displayed significant cytotoxicity against NCI-H226 with an IC_{50} value of 12.00 μM (Chen et al., 2018).

Fissistigma fulgens (Hook.f. & Thomson) Merr., a woody climber native to the lowland forests of Thailand and Southeast Asia, has been scarcely investigated, with only one phytochemical report to date (Hadi, 2000). Given the abundance of biologically active chalcones and dihydrochalcones in *Fissistigma* species, *F. fulgens* represents a promising yet underexplored source of bioactive natural products. This study investigates the leaf constituents of *F. fulgens*, focusing on the isolation, structural characterization, and evaluation of their biological activities. The findings expand the phytochemical knowledge of the genus *Fissistigma* and may lead to the discovery of compounds with potential pharmaceutical relevance.

2. Results and discussion

The EtOAc extract of *F. fulgens* leaves was subjected to various chromatographic techniques, including silica gel, C18 reversed-phase, and Sephadex LH-20 column chromatography, followed by HPLC. This led to the isolation of two previously undescribed dimeric dihydrochalcones **1** and **2**, three previously undescribed monomeric chalcones (**3**–**5**), and three known compounds: pinostrobin (**6**) (Kurkina et al., 2013), 5-hydroxy-3′,4′,7-trimethoxyflavone (**7**) (Sudha and Srinivasan, 2014), and velutin (**8**) (Kang et al., 2011) (see Fig. 1).

2.1. Structural elucidation

Fissisfulgenone A (**1**) was obtained as yellow crystals. Its molecular formula was established to be $C_{50}H_{42}O_{12}$ based on the ^{13}C NMR and HRESIMS data [*m/z* 835.2748 $[M + H]^+$ (calcd for $C_{50}H_{43}O_{12}$, 835.2749)]. The UV spectrum displayed typical absorption maxima of a dihydrochalcone derivative at 266, 291, and 354 nm (Jaidee et al., 2019; Lan et al., 2011). The IR spectrum displayed the presence of hydroxy (3504 cm^{-1}) and carbonyl (1635 cm^{-1}) functionalities. Single-crystal X-ray diffraction (CCDC 2448392, Fig. 3) established its symmetrical dimeric structure, with two dihydrochalcone monomers linked through a C-2"–C-2a" bond. The ^1H NMR data (Table 1) associated with HSQC data assigned the ^1H and ^{13}C resonances of the dihydrochalcone core structure as follows: a set of monosubstituted aromatic ring systems [δ_H 7.30 (4H, m)/δ_C 128.5, C-2/C-2a and C-6/C-6a, δ_H 7.22 (2H, m)/δ_C 126.2, C-4/C-4a, and δ_H 7.12 (4H, m)/δ_C 128.4, C-3/C-3a and C-5/C-5a], diastereotopic methylene groups [δ_H 2.99 (2H, ddd, *J* = 15.3, 8.9, 6.2 Hz) and 2.90 (2H, ddd, *J* = 15.7, 8.9, 6.4 Hz)/δ_C 44.3, C-8/C-8a and δ_H 2.70 (2H, ddd, *J* = 15.4, 8.9, 6.4 Hz) and 2.58 (2H, m)/δ_C 30.4, C-7/C-7a], methoxy groups [δ_H 4.05 (6H, s)/δ_C 59.7, 4′-OMe/4a'OMe], hydrogen-bonded hydroxy protons [δ_H 13.24 (2H, s, 2′-OH/2a′-OH)], and hydroxy protons [δ_H 5.20 (2H, s, 3′-OH/3a′-OH)]. In addition, the benzyl unit displayed resonances at δ_H 7.06 (2H, m)/δ_C 127.2, C-7"/C-7a", δ_H 7.06 (4H, m)/δ_C 128.0, C-6"/C-6a" and C-8"/C-8a", δ_H 6.86 (4H, m)/δ_C 130.3, C-5"/C-5a" and C-9"/C-9a", and δ_H 4.08 (2H, d, *J* = 13.0 Hz) and 3.75 (2H, d, *J* = 13.0 Hz)/δ_C 37.2, C-3"/C-3a"]. The linkage of both units was confirmed by the HMBC correlations (Fig. 2) between H_2-3"/H_2-3a" with C-5′/C-5a′, C-1"/C-1a", C-4"/C-4a", C-5"/C-5a" and C-9"/C-9a". Finally, the absence of a proton signals for H-2"/H-2a", together with the HMBC correlations between H-3"/H-3a" with C-2"/C-2a", indicated that two monomers must be directly connected through C-2"–C-2a". Compound **1** was further analyzed and resolved by chiral-phase HPLC to yield (−)-**1** [t_R 6.1 min, $[\alpha]_D^{25}$ −122 (*c* 0.5, MeOH)] and (+)-**1**[t_R 7.3 min, $[\alpha]_D^{25}$ +118 (*c* 0.5, MeOH)] (Fig. S36). The ECD curve of (−)-**1** showed a positive Cotton effect at ca. 297 nm and a negative Cotton effect at ca. 211, 254, and 355 nm, whereas (+)-**1** had opposite Cotton effects at the aforementioned wavelengths (Fig. 4). The calculated ECD spectra of (2″*S*,2a″*S*)-**1** and (2″*R*,2a″*R*)-**1** were matched well with the experimental ECD spectra of (−)-**1** and (+)-**1**, respectively. Therefore, the names of (−)-(2″*S*,2a″*S*)-*fissisfulgenone* A and (+)(2″*R*,2a″*R*)-*fissisfulgenone* A were assigned.

Fissisfulgenone B (**2**), obtained as a yellow amorphous powder, was found to possess the same molecular formula ($C_{50}H_{42}O_{12}$) as fissisfulgenone A (**1**), as determined by its positive HRESIMS ion at *m/z* 835.2780 $[M + H]^+$ (calcd for $C_{50}H_{43}O_{12}$, 835.2749). Detailed comparison of NMR data (Table 1) indicated that compound **2** was the C-2a" epimer of compound **1**. The slight chemical shift differences observed in the methylene protons - H_2-7/H_2-7a [δ_H 2.68 (4H, m)], H_2-8/H_2-8a [δ_H 3.00 (4H, m)], and H_2-3"/H_2-3a" [δ_H 3.99 (2H, d, *J* = 13.1 Hz) and 3.94

Table 1
^1H (500 MHz) and ^{13}C (125 MHz) NMR spectroscopic data of compounds **1** and **2** in $CDCl_3$.

Position	**1**		**2**	
	δ_C	δ_H, mult (*J* in Hz)	δ_C	δ_H, mult (*J* in Hz)
1/1a	140.4	–	140.3	–
2/2a, 6/6a	128.5	7.30 m	128.5	7.24 m
3/3a, 5/5a	128.4	7.12 m	128.4	7.24 m
4/4a	126.2	7.22 m	126.2	7.17 m
7/7a	30.4	2.70 ddd (15.4, 8.9, 6.4); 2.58 m	30.5	2.68 m
8/8a	44.3	2.99 ddd (15.3, 8.9, 6.2); 2.90 ddd (15.7, 8.9, 6.4)	44.5	3.00 m
9/9a	203.1	–	203.5	–
1′/1a′	100.6	–	100.9	–
2′/2a′	152.2	–	152.4	–
3′/3a′	130.6	–	131.7	–
4′/4a′	146.9	–	148.3	–
5′/5a′	108.5	–	107.6	–
6′/6a′	145.3	–	146.4	–
2′-OH/2a′-OH	–	13.24 s	–	13.32 s
3′-OH/3a′-OH	–	5.20 s	–	5.37 s
4′-OMe/4a′-OMe	59.7	4.05 s	60.4	4.12 s
1"/1a"	173.6	–	174.8	–
2"/2a"	56.9	–	61.8	–
3"/3a"	37.2	4.08 d (13.0); 3.75 d (13.0)	35.0	3.99 d (13.1); 3.94 d (13.1)
4"/4a"	134.5	–	134.9	–
5"/5a", 9"/9a"	130.3	6.86 m	130.0	6.98 m
6"/6a", 8"/8a"	128.0	7.06 m	128.3	7.09 m
7"/7a"	127.2	7.06 m	127.3	7.09 m

(2H, d, $J = 13.1$ Hz)] - along with the downfield shift of the quaternary carbon C-2a" by 4.9 ppm (Table 1), provide additional support for the proposed structure. The key COSY and HMBC correlations confirming the structure of compound **2** are illustrated in Fig. 2. Like compound **1**, it was resolved into (−)-**2** (t_R 5.8 min) and (+)-**2** (t_R 6.9 min) by chiral-phase HPLC (Fig. S37). The experimental ECD spectrum of (−)-**2** showed sequential negative and positive Cotton effects at 206, 253, 297, and 341 nm, which closely matched the calculated spectrum for the (2"*S*,2a"*R*) enantiomer. In contrast, the ECD spectrum of (+)-**2** corresponded to its mirror image (Fig. 4). Accordingly, the absolute configurations of (−)-**2** and (+)-**2** were assigned as (−)-(2"*S*,2a"*R*)-fissisfulgenone B and (+)-(2"*R*,2a"*S*)-fissisfulgenone B, respectively.

Fissisfulgenone C (**3**) was isolated as a yellow amorphous powder. The molecular formula $C_{28}H_{26}O_7$ from the molecular ion peak at *m/z* 475.1749 $[M + H]^+$ (calcd for $C_{28}H_{27}O_7$, 475.1751) in the HRESIMS spectrum, accompanied by 28 carbon resonances (Table 2) indicated that compound **2** was a monomeric dihydrochalcone. NMR data (Table 2) revealed a dihydrochalcone skeleton similar to **1** and **2**, but with a 2-oxopropyl substituent [(δ_H 3.23 (1H, d, $J = 13.0$ Hz) and 3.06 (1H, d, $J = 13.0$ Hz)/δ_C 49.6, C-10"), δ_H 2.11 (3H, s)/δ_C 29.5, C-12"), and δ_C 204.6, C-11"]. HMBC correlations [H_2-12 to C-5′ (δ_C 108.9), C-1" (δ_C 178.1), C-2" (δ_C 50.5), C-11", and C-12"] confirmed the location of the 2-oxopropyl side chain at C-2". The chiral-phase HPLC resolution of compound **3** afforded two enantiomers: (+)-**3** (t_R 6.8 min) and (−)-**3** (t_R 8.9 min) (Fig. S38). The absolute configurations of (+)-**3** and (−)-**3** were established as (2"*R*) and (2"*S*), respectively, by the comparison of their experimental and calculated ECD data (Fig. 4). Hence, the structures of (+)-(2"*R*)-fissisfulgenone C and (−)-(2"*S*)-fissisfulgenone C, were established.

Fissisfulgenone D (**4**), yellow amorphous powder, gave an $[M + H]^+$ ion at *m/z* 417.1335 in the HRESIMS spectrum corresponding to a molecular formula of $C_{25}H_{20}O_6$. Compound **4** exhibited a structure closely related to compound **3** but lacked the 2-oxopropyl group. Instead, a benzylidene moiety was present, confirmed by characteristic NMR resonances [δ_H 8.16 (1H, s)/δ_C 142.7, C-3", δ_H 8.01 (2H, m)/δ_C 131.5, C-5"/C-9", δ_H 7.45 (2H, m)/δ_C 128.4, C-6"/C-8", and δ_H 7.45 (1H, m)/δ_C 130.7, C-7"] (Table 2) and HMBC correlations [H-3" to C-5′ (δ_C 107.7), C-1" (δ_C 164.8), C-2" (δ_C 119.2), C-4" (δ_C 133.8), C-5" and C-9"] (Fig. 2) confirmed the location of the benzylidene group at C-2".

Fissisfulgenone E (**5**) was obtained as a yellow amorphous powder, with a molecular formula of $C_{26}H_{22}O_7$ from HRESIMS at *m/z* 445.1302 $[M - H]^-$ (calcd for $C_{26}H_{21}O_7$, 445.1293), and also possessed a dihydrochalcone core. Unlike the other dihydrochalcones, it contained a furan ring substituted with a methyl ester [δ_H 3.96 (3H, s)/δ_C 52.7, 3″-OMe and δ_C 165.6, C-9″] and a phenyl group [δ_H 7.71 (2H, m)/δ_C 126.7, C-3″/C-7″, δ_H 7.40 (1H, m)/δ_C 129.4, C-5″, δ_H 7.40 (2H, m)/δ_C 128.8, C-4″/C-6″, and δ_C 129.0, C-2″], as supported by NMR data (Table 3). The HMBC correlations of H-3″ and H-7″ with C-1″ and C-2″ (Fig. 2) confirmed the location of the phenyl moiety, and then, the methyl ester was placed at C-8″.

The proposed biosynthetic pathway for compounds **1** and **2** is illustrated in Fig. 5. Compound **4** may originate from a hybrid of chalcone and cinnamic acid (Lan et al., 2005). Reductive activation of compound **4** via a radical process at the $\Delta^{2''}$ double bond generates radical intermediate A. Subsequently, the intermediate An undergoes carbon-carbon oxidative radical-radical coupling with itself, leading to the formation of the dimeric structures **1** and **2**. Importantly, the radical-radical coupling of two units of A can occur from either face of the radical center, thereby yielding enantiomeric dimers.

2.2. Cytotoxicity of compounds 1, 3, and 4

The cytotoxic activities (Table 4) of compounds **1**, **3**, and **4** were evaluated against five human cancer cell lines, including MDA-MB231 (human breast adenocarcinoma), A549 (human lung carcinoma), Huh7 (human hepatocellular carcinoma), SW480 (human colorectal adenocarcinoma), and HT29 (human colorectal adenocarcinoma), using the MTT assay. Compounds **3** and **4** showed cytotoxic activity against all cancer cell lines, whereas compound **1** was inactive ($IC_{50} > 100$ μM). Compound **3** (40.6 ± 5.31 μM) exhibited stronger activity against SW480 cells compared to compound **4** (61.9 ± 2.80 μM), while compound **4** was more potent against A549 (38.2 ± 1.23 μM) and Huh7 (21.2 ± 6.18 μM) cells. Although both compounds **3** and **4** exhibited anticancer potential, their cytotoxic activities were generally lower than that of the commercial chemotherapeutic agent cisplatin across four cancer cell lines, with the exception of A549 lung carcinoma cells. In A549 cells, compounds **3** and **4** demonstrated slightly stronger cytotoxic effects, with IC_{50} values of 60.7 and 38.2 μM, respectively, compared to 70.6 μM for cisplatin. Notably, both compounds **3** and **4** outperformed paclitaxel in A549 and SW480 assays, and compound **4** was also more effective than cisplatin in A549 cells. Though all tested compounds contained methoxy groups, only compounds **3** and **4** exhibited cytotoxicity, suggesting that the dimeric structure and molecular size of compound **1** may limit cellular uptake and biological activity.

2.3. Anti-viral effect of compounds 1, 3, and 4 against DENV-infected Huh7

Virus production from DENV-infected Huh7 cells was not affected by treatment with either compounds **3** or **4** at any concentration, as

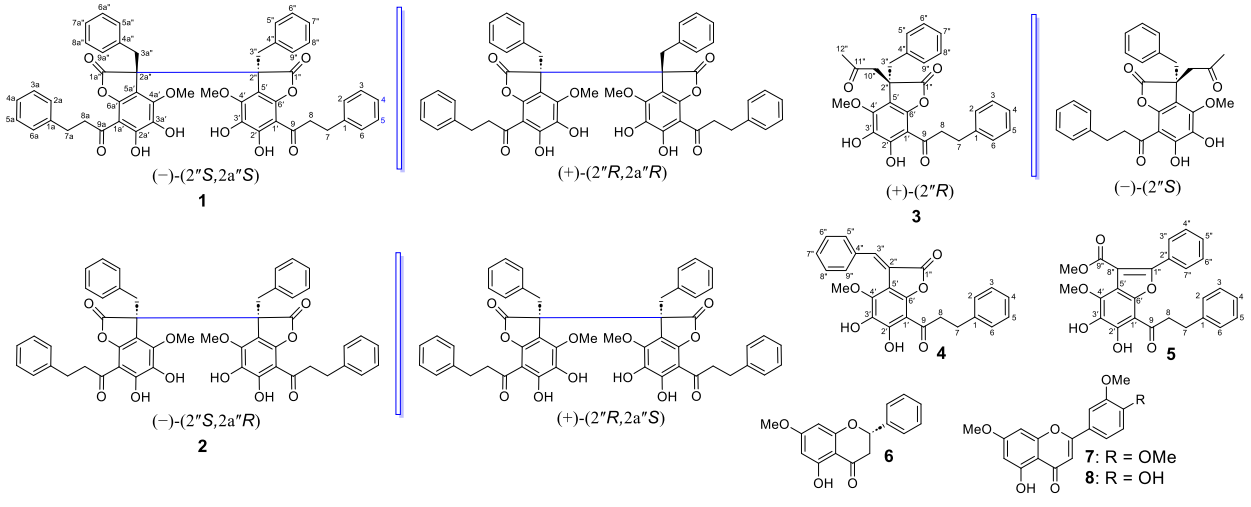

Fig. 1. Isolated compounds from the leaves of *F. fulgens*.

represented by the viral foci shown in Fig. 6A. Interestingly, the non-toxic concentration of compound **1** (50 μM) clearly reduced viral foci formation (Fig. 6A). Moreover, the measured viral titer was significantly reduced from 1.29×10^6 FFU/mL in untreated cells to 1.30×10^5 FFU/mL in treated cells (Fig. 6B), which correlated with the previous viral foci result. In comparison, treatment with positive control, ribavirin (RV), at 100 μM almost completely suppressed virus production, as shown in Fig. 6A and 6B. Among the three structurally related compounds, **1** and **3**–**4**, only compound **1** exhibited antiviral activity that may correlate to its dimeric structure. To clarify the stage of the viral life cycle targeted by compound **1**, time-of-addition and time-of-elimination assays should be conducted. As there is currently no effective treatment for DENV infection (Low et al., 2017), our findings highlight compound **1** as a promising lead compound for alternative therapy. To advance compound **1** toward clinical application, further studies involving chemical optimization, in vivo toxicity, and clinical validation are imperative.

2.4. Anti-inflammatory effect of compounds *1*, *3*, and *4* against LPS-induced inflammation

Representative phase-contrast micrographs revealed that stimulation with LPS induced pronounced morphological changes in RAW264.7 macrophages. These cells displayed an irregular, spread-out morphology with extended pseudopodia, characteristic of macrophage activation. In contrast, pretreatment with compounds **1** and **3** preserved a more regular, rounded morphology with reduced pseudopodia formation, as shown in Fig. 7A. These results indicate that compound **1**, and particularly compound **3**, can attenuate LPS-induced morphological alterations associated with macrophage activation. To further validate the anti-inflammatory effects of the tested compounds, the Griess assay was performed. As illustrated in Fig. 7B, all tested compounds significantly reduced NO production in a dose-dependent manner. Compound **3** exhibited the most potent effect, reducing NO levels by approximately 80 % at 10 μM (a 5-fold reduction compared to the LPS group, $IC_{50} = 5.27 \pm 0.11$ μM). Compound **1** reduced NO by ~72 % at 50 μM (3.6-fold, $IC_{50} = 27.85 \pm 0.63$ μM), while compound **4** achieved ~48 % inhibition at 10 μM (1.9-fold, $IC_{50} = 9.44 \pm 0.14$ μM). Thus, compound **3** demonstrated the strongest anti-inflammatory activity, as evidenced by its ability to suppress LPS-induced NO production and maintain normal macrophage morphology. These findings are consistent with previous reports showing that LPS induces morphological changes associated with macrophage activation (Pi et al., 2014; Saxena et al., 2003). Although compound **3** reduced NO levels by up to 80 %, its cytotoxic concentration (CC_{50}) was 60.29 μM (Table 5). In contrast, compound **1** achieved comparable inhibitory effects at higher, non-cytotoxic concentrations ($CC_{50} > 100$ μM), suggesting that compound **1** may also be a promising anti-inflammatory candidate.

3. Conclusions

This study reports the first comprehensive phytochemical analysis of *F. fulgens* leaves, leading to the discovery of five previously undescribed dihydrochalcone derivatives—two dimeric and three monomeric compounds. Structural elucidation was accomplished using spectroscopic techniques, with single-crystal X-ray diffraction further confirming the unique symmetrical dimeric structure of fissisfulgenone A. Enantiomeric separation and absolute configuration assignment were successfully achieved for compounds **1**–**3** via chiral-phase HPLC and ECD analysis. Biological evaluation revealed that fissisfulgenones C and D exhibited moderate cytotoxic effects against a panel of human cancer cell lines, while fissisfulgenone A demonstrated notable anti-DENV activity and nitric oxide inhibition at non-cytotoxic doses. These findings not only broaden the chemical diversity of chalcones within the Annonaceae family but also underscore the potential of *F. fulgens* as a promising source of bioactive compounds for future pharmaceutical development. Further investigations into structure–activity relationships and in vivo efficacy are warranted to advance these compounds toward therapeutic application.

4. Experimental

4.1. General experimental procedures

The melting point was measured on a BUCHI Melting Point M-560 apparatus. The Optical rotations were measured using a Jasco P-2000 polarimeter. Electronic circular dichroism (ECD) spectra were recorded on a JASCO J-1500 spectrophotometer. UV absorption spectra were obtained using a Cary 5000 UV–Vis–NIR spectrophotometer, and IR spectra were acquired with a PerkinElmer FTS FT-IR spectrometer. NMR spectra were recorded on a Bruker AV-500 spectrometer operating at 500 MHz, with tetramethylsilane (TMS) as the internal standard. The X-ray crystallography was performed on a Rigaku SuperNova diffractometer equipped with a HyPix 3000 detector using Cu Kα radiation.

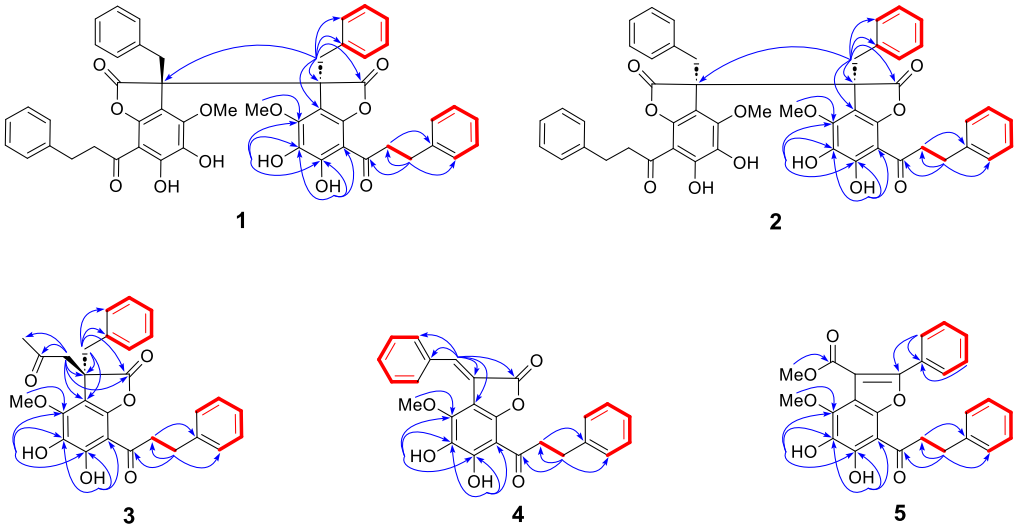

Fig. 2. ^1H–^1H COSY (red, bold), selected HMBC (blue single arrows) correlations of compounds **1**–**5**. (For interpretation of the references to color in this figure legend, the reader is referred to the Web version of this article.)

HRESIMS data were obtained using an Agilent LC-QTOF 6500 system coupled with an Agilent ZORBAX Eclipse Plus C18 column (2.1 × 50 mm, 1.8 μm). HPLC separations were carried out on an Agilent 1260 Infinity II system with a Diode Array Detector HS, using a reversed-phase C18 (RP C18) CSC-Inertsil 150A/ODS-2 column (25 × 0.94 cm) and a CHIRALCEL OD-H column (4.6 × 250 mm). Silica gel C60 (0–20 μm, SiliCycle® Inc.) and Sephadex LH-20 were employed for column chromatography. Thin-layer chromatography (TLC) was performed on pre-coated silica gel 60 F_{254} plates, and spots were visualized under UV light at 254 and 310 nm.

4.2. Plant material

The leaves of *F. fulgens* were collected in October 2021 from Narathiwat Province (N: 6.156754°, E: 101.664661°), Thailand. This plant was identified Mr. Abdulromea Baka. A voucher specimen (MFU-NPR219) was deposited at the Natural Products Research Laboratory of Mae Fah Luang University.

4.3. Extraction and isolation

The air-dried leaves of *F. fulgens* (1.5 kg) were extracted with EtOAc (2 × 5 L, for 3 days) at room temperature. The solvent was removed by rotatory evaporation, under reduced pressure, yielding 52.9 g of extract. The EtOAc extract was further fractionated using a C_{18} reverse-phase column chromatography (CC) (3:2 v/v, MeOH/H_2O) to give five fractions (Fr. FGL1–FGL5). Fraction FGL3 (5.4 g) was further separated by CC over silica gel (2:3 v/v, EtOAc/hexanes) to afford six subfractions (Fr. FGL3A–FGL3F). Subfraction FGL3B (162.0 mg) was purified by CC over silica gel (2:3 v/v, EtOAc/hexanes) to give **4** (18.2 mg) and two subfractions (Fr. FGL3BA–FGL3BB). Compounds **6** (0.7 mg), **7** (0.7 mg), and **8** (0.9 mg) and three fractions (Fr. FGL3BAa–FGL3BAc) were obtained from subfraction FGL3BA (18.7 mg) by repeated CC over Sephadex LH-20 (4:1 v/v, MeOH/CH_2Cl_2). Subfraction FGL3C (219.5 mg) was fractioned by CC over Sephadex LH-20 (4:1 v/v, MeOH/CH_2Cl_2) to obtain four subfractions (Fr. FGL3CA–FGL3CD). Subfraction FGL3CB (35.2 mg) was chromatographed by CC over silica gel (1.5:3.5 v/v, EtOAc/hexanes) to obtain **1** (15.0 mg) and two subfractions (Fr. FGL3CBa–FGL3CBb). Compound **2** (0.9 mg, t_R 22.3 min) was purified from subfraction FGL3CBa (5.1 mg) by RP C_{18} HPLC (3.5:1.5 v/v, CH_3CN/H_2O, 1.0 mL/min). Subfraction FGL3CC (65.7 mg) was chromatographed by CC over silica gel (2:3 v/v, acetone/hexanes) to obtain **3** (5.1 mg) and two subfractions (Fr. FGL3CCa–FGL3CCb). Purification of subfraction FGL3CCb (18.0 mg) by CC over silica gel (2:3 v/v, EtOAc/hexanes) to yield **5** (0.8 mg).

4.3.1. Fissisfulgenone A (1)

Yellow crystals: m.p. 158–160 °C; $[\alpha]_D^{25}$ +5.7 (*c* 0.5, MeOH); UV (MeOH) λ_{max} (log ε) 266 (4.7), 291 (4.7), and 354 (4.1) nm; IR (neat) ν_{max} 3504, 2923, 1804, 1635, 1425, 1261, 1005, and 790 cm^{-1}; ^1H and ^{13}C NMR, see Table 1; HRESIMS *m/z* 835.2748 $[M + H]^+$ (calcd for $C_{50}H_{43}O_{12}$, 835.2749).

Chiral-phase HPLC resolution and ECD data of (−)-**1** and (+)-**1**.

Resolution of compound **1** was performed by semi-preparative HPLC on a chiral column (CHIRALCEL OD-H, flow rate 1.0 mL/min, *n*-hexane/*i*PrOH, 3:2 v/v).

Compound (−)-(2"*S*, 2a"*S*)-**1** [(t_R = 6.1 min), $[\alpha]_D^{25}$ −122 (*c* 0.5, MeOH)]; ECD (MeOH) λ_{max} ($\Delta\varepsilon$) 211 (−0.20), 254 (−0.12), 297 (+0.02), 355 (−0.02) nm.

Compound (+)-(2"*R*, 2a"*R*)-**1** [(t_R = 7.3 min), $[\alpha]_D^{25}$ +118 (*c* 0.5, MeOH)]; ECD (MeOH) λ_{max} ($\Delta\varepsilon$) 211 (+0.20), 254 (+0.12), 297 (−0.02), 355 (+0.02) nm.

4.3.2. Fissisfulgenone B (2)

Yellow amorphous powder: $[\alpha]_D^{25}$ −6.4 (*c* 0.5, MeOH); UV (MeOH) λ_{max} (log ε) 264 (3.9), 291 (3.9), and 355 (3.5) nm; IR (neat) ν_{max} 3501, 2923, 1804, 1636, 1425, 1261, 1004, and 786 cm^{-1}; ^1H and ^{13}C NMR, see Table 1; HRESIMS *m/z* 835.2780 $[M + H]^+$ (calcd for $C_{50}H_{43}O_{12}$, 835.2749).

Chiral-phase HPLC resolution and ECD data of (−)-**2** and (+)-**2**.

Resolution of compound **2** was performed by semi-preparative HPLC on a chiral column (CHIRALCEL OD-H, flow rate 1.0 mL/min, *n*-hexane/*i*PrOH, 3:2 v/v).

Compound (−)-(2"*S*, 2a"*R*)-**2** [(t_R = 5.8 min), $[\alpha]_D^{25}$ −93 (*c* 0.5, MeOH)]; ECD (MeOH) λ_{max} ($\Delta\varepsilon$) 206 (−0.03), 253 (−0.01), 297 (+0.01), 341 (−0.01) nm.

Compound (+)-(2"*R*, 2a"*S*)-**2** [(t_R = 6.9 min), $[\alpha]_D^{25}$ +93 (*c* 0.5, MeOH)]; ECD (MeOH) λ_{max} ($\Delta\varepsilon$) 212 (+0.20), 262 (+0.01), 299 (−0.01), 355 (+0.01) nm.

4.3.3. Fissisfulgenone C (3)

Yellow amorphous powder: $[\alpha]_D^{25}$ +3.6 (*c* 0.5, MeOH); UV (MeOH) λ_{max} (log ε) 258 (4.8), 289 (4.9), and 360 (4.6) nm; IR (neat) ν_{max} 3409, 2924, 1776, 1632, 1424, 1347, 1267, 1005, and 750 cm^{-1}; ^1H and ^{13}C NMR, see Table 2; HRESIMS *m/z* 475.1749 $[M + H]^+$ (calcd for $C_{28}H_{27}O_7$, 475.1751).

Chiral-phase HPLC resolution and ECD data of (+)-**3** and (−)-**3**.

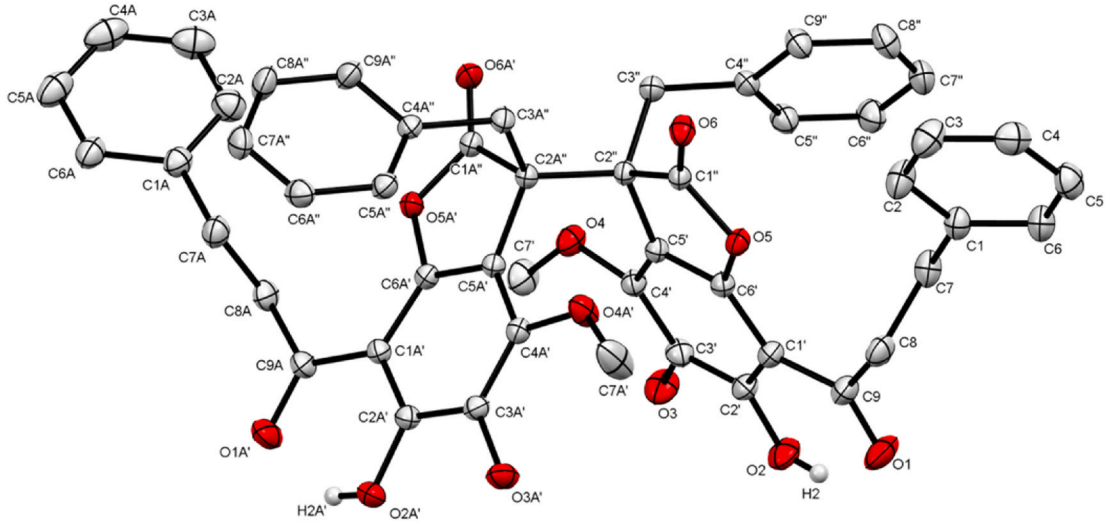

Fig. 3. X-ray ORTEP-like of compound **1**.

Resolution of compound **3** was performed by semi-preparative HPLC on a chiral column (CHIRALCEL OD-H, flow rate 1.0 mL/min, *n*-hexane/*i*PrOH, 3:2 v/v).

Compound (+)-(2"*R*)-**3** [(t_R = 6.8 min), $[\alpha]_D^{25}$ +139 (*c* 0.5, MeOH)]; ECD (MeOH) λ_{max} ($\Delta\varepsilon$) 212 (−0.46), 253 (+0.08), 280 (−0.03), 301 (+0.01) nm.

Compound (−)-(2"*S*)-**3** [(t_R = 8.9 min), $[\alpha]_D^{25}$ −139 (*c* 0.5, MeOH)]; ECD (MeOH) λ_{max} ($\Delta\varepsilon$) 213 (+0.44), 255 (−0.08), 278 (+0.03), 298 (−0.02) nm.

4.3.4. *Fissisfulgenone D* (*4*)

Yellow amorphous powder: UV (MeOH) λ_{max} (log ε) 259 (4.8), 289 (4.9), and 362 (4.6) nm; IR (neat) ν_{max} 3445, 2924, 1805, 1636, 1425, 1349, 1269, and 1025 cm^{-1}; ^1H and ^{13}C NMR, see Table 2; HRESIMS *m/z* 417.1335 $[M + H]^+$ (calcd for $C_{25}H_{21}O_6$, 417.1333).

4.3.5. *Fissisfulgenone E* (*5*)

Yellow amorphous powder: UV (MeOH) λ_{max} (log ε) 271 (4.6), 293 (4.6), and 352 (4.0) nm; IR (neat) ν_{max} 3376, 2923, 1716, 1626, 1457, 1354, 1260, and 1169 cm^{-1}; ^1H and ^{13}C NMR, see Table 3; HRESIMS *m/z* 445.1302 $[M - H]^-$ (calcd for $C_{26}H_{21}O_7$, 445.1293).

4.4. *X-ray crystal structure analysis of compound* ***1***

Single crystals of compound **1** ($C_{50}H_{42}O_{12}$) were crystallized in methanol upon slow evaporation under ambient conditions. A suitable single crystal was selected and mounted on a Rigaku SuperNova diffractometer with a HyPix 3000 detector using Cu Kα radiation (λ = 1.54184 Å) at 293(2) K. Data reduction, scaling, and absorption corrections were performed using CrysAlisPro (version 1.171.40.84a). The

Table 2
^1H (500 MHz) and ^{13}C (125 MHz) NMR spectroscopic data of compounds **3** and **4** in $CDCl_3$.

Position	**3**		**4**	
	δ_C	δ_H, mult (*J* in Hz)	δ_C	δ_H, mult (*J* in Hz)
1	140.6	–	140.6	–
2/6	128.6	7.16 m	128.5	7.30 m
3/5	128.4	7.28 t (7.4)	128.6	7.31 m
4	126.1	7.20 m	126.2	7.21 ddd (8.1, 4.8, 4.1)
7	30.4	2.74 dddd (22.9, 14.0, 8.6, 6.6)	30.1	3.06 t (7.5)
8	44.4	3.11 m	44.5	3.45 t (7.5)
9	203.7	–	203.7	–
1′	101.7	–	101.9	–
2′	151.5	–	152.4	–
3′	131.7	–	132.2	–
4′	147.0	–	147.3	–
5′	108.9	–	107.7	–
6′	146.5	–	146.6	–
2′-OH	–	13.17 s	–	13.51 s
3′-OH	–	5.39 br s	–	5.46 br s
4′-OMe	60.7	4.26 s	60.7	4.28 s
1"	178.1	–	164.8	–
2"	50.5	–	119.2	–
3"	42.3	3.69 d (18.3); 3.25 d (18.3)	142.7	8.16 s
4"	134.1	–	133.8	–
5"/9"	129.5	6.86 m	131.5	8.01 m
6"/8"	128.1	7.07 m	128.4	7.45 m
7"	127.3	7.07 m	130.7	7.45 m
10"	49.6	3.23 d (13.0); 3.06 d (13.0)	–	–
11"	204.6	–	–	–
12"	29.5	2.11 s	–	–

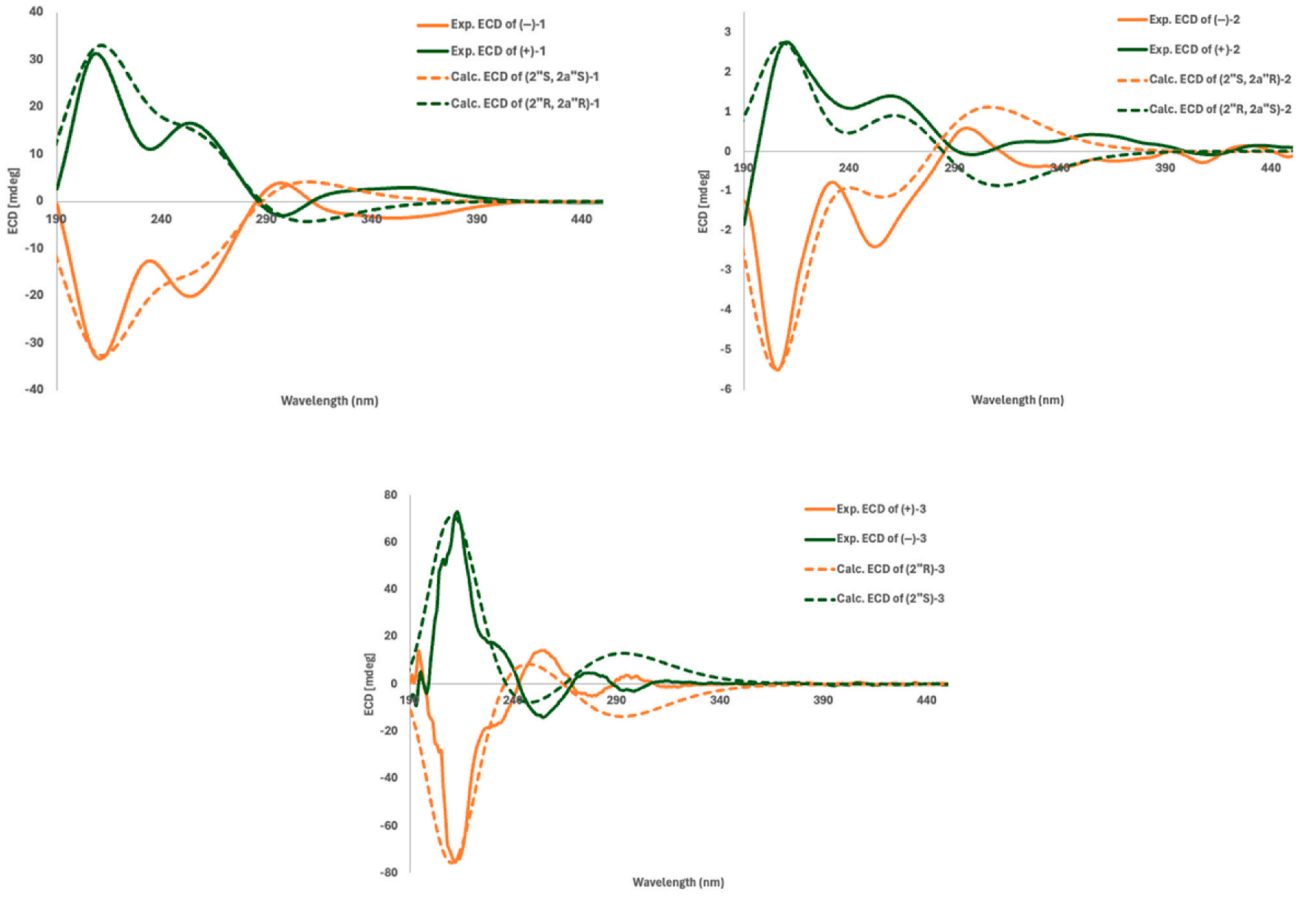

Fig. 4. Experimental and calculated ECD spectra of compounds **1**−**3**.

Table 3
^{1}H (500 MHz) and ^{13}C (125 MHz) NMR spectroscopic data of compound **5** in $CDCl_3$.

Position	**5**	
	δ_C	δ_H, mult (*J* in Hz)
1	140.6	–
2/6	128.3	7.28 m
3/5	128.5	7.28 m
4	126.3	7.22 m
7	30.1	3.15 m
8	44.1	3.67 m
9	202.9	–
1′	102.3	–
2′	152.5	–
3′	133.4	–
4′	144.5	–
5′	109.5	–
6′	146.6	–
2′-OH	–	13.63 s
3′-OH	–	5.56 br s
4′-OMe	61.0	4.16 s
1"	152.8	–
2"	129.0	–
3"/7"	126.7	7.71 m
4"/6"	128.8	7.40 m
5"	129.4	7.40 m
8"	113.1	–
9"	165.6	–
3"-OMe	52.7	3.96 s

structure was solved, and the space group P-1 was determined by intrinsic phasing using ShelXT and refined by full-matrix least-squares minimization on F2 using SHELXL (Sheldrick, 2015a, 2015b) with OLEX2 (Dolomanov et al., 2009) as a graphical interface. All non-hydrogen atoms were refined anisotropically. The crystallographic data for **1** (CCDC 2448392) can be obtained free of charge from the Cambridge Crystallographic Data Centre *via* www.ccdc.cam.ac.uk/data_request/cif.

Crystal Data for **1**: yellow block-shaped crystals, $C_{50}H_{42}O_{12}$ (M = 834.83 g/mol): triclinic, space group P-1 (no. 2), a = 11.6450(2) Å, b = 12.2011(2) Å, c = 16.3229(3) Å, α = 69.925(2)°, β = 77.5140(10)°, γ = 86.5980(10)°, V = 2126.49(7) Å^3, Z = 2, T = 293(2) K, μ(Cu Kα) = 0.768 mm^{-1}, ρ_{calc} = 1.304 g/cm^3, 20703 reflections measured (5.894° ≤ 2θ ≤ 137.17°), 7767 unique (R_{int} = 0.0706, R_{sigma} = 0.0678) which were used in all calculations. The final R_1 was 0.0540 (I > 2σ(I)) and wR_2 was 0.1564 (all data).

4.5. Computational method

The absolute configurations of **1**–**3** were determined by quantum chemical calculation of ECD spectra using Gaussian 09 software (Frisch et al., 2009). The stereoisomer was geometrically optimized using the TDDFT method at the B3LYP/6-31+G(d) level in gas phase to afford a preferred conformer. The ECD spectrum was calculated using the TDDFT method at the TDDFT/B3LYP/6-31+G(d,p) level.

4.6. Cytotoxicity assay

The cytotoxicity of compounds **1**, **3**, and **4** was investigated in five cancer cell lines consisting of MDA-MB231 (breast cancer), A549 (lung cancer), Huh7 (liver cancer), SW480 (colorectal cancer), and HT29 (colorectal cancer). These human cell lines were kindly supported by School of Medicine, Mae Fah Luang University, Thailand, and the Laboratory of Biochemistry, Chulabhorn Research Institute, Thailand. All cells were cultured in DMEM medium, supplemented with 10 % heat-inactivated fetal bovine serum (FBS) and 1 % penicillin-streptomycin-amphotericin-B solution (Gibco, USA). The cytotoxicity activity was determined using MTT assay (Saharat et al., 2025). Cells were plated into 96-well plates at a density 1 × 10^4 cells/well and incubated overnight at 37 °C in a humidified incubator with 5 % CO_2. Then cells were treated with either compound or standard chemotherapy control (paclitaxel or cisplatin (MedChemExpress, USA)) for 24 h, in which untreated control cells were exposed to 0.5 % DMSO. Following this, the culture media was replaced with media containing with 0.5 mg/ml MTT and incubated for 2 h. Then media was replaced by 100 μl of DMSO and the absorbance was determined at 570 nm using a microplate reader. The IC_{50} of the compound and chemotherapy was calculated using an online calculator tool: AAT Bioquest, Inc. (Pleasanton, CA, USA); Available online: https://www.aatbio.com/tools/ic50-calculator.

4.7. Anti-viral assay

The antiviral assays were performed using dengue virus (DENV) infection of the human liver cell line, Huh7 cells, as previously described (Morchang et al., 2021). Briefly, Huh7 cells were seeded into 24-well

Table 4
Cytotoxicity of compounds against human cancer cell lines.

Compounds	IC_{50} (μM)				
	MDA-MB231	A549	Huh7	SW480	HT29
1	>100	>100	>100	>100	>100
3	49.9 ± 22.9	60.7 ± 14.7	28.1 ± 2.95	40.6 ± 5.31	68.0 ± 12.0
4	48.7 ± 8.28	38.2 ± 1.23	21.2 ± 6.18	61.9 ± 2.80	73.1 ± 0.19
Paclitaxel	1.76	>100	0.15	>100	0.03
Cisplatin	19.6	70.6	16.5	33.4	29.8

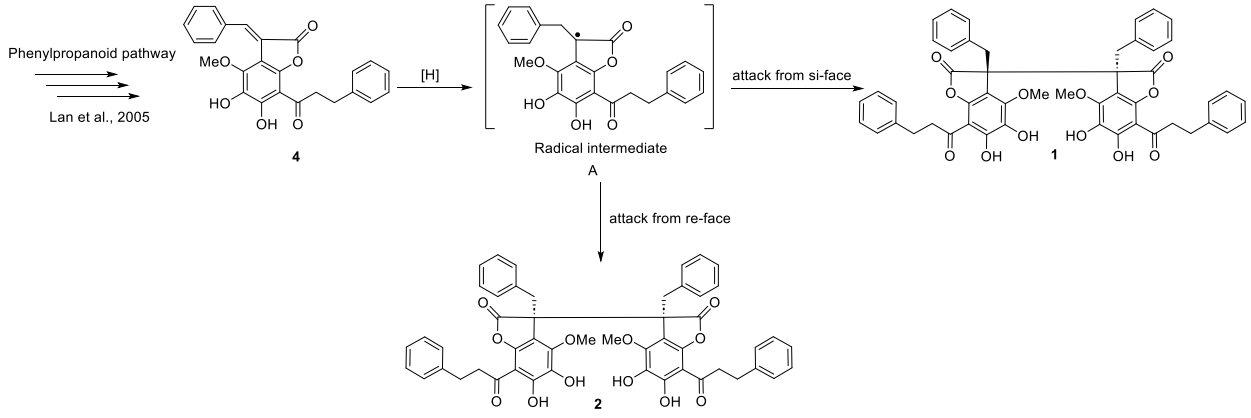

Fig. 5. A plausible biosynthetic pathway of compounds **1** and **2**.

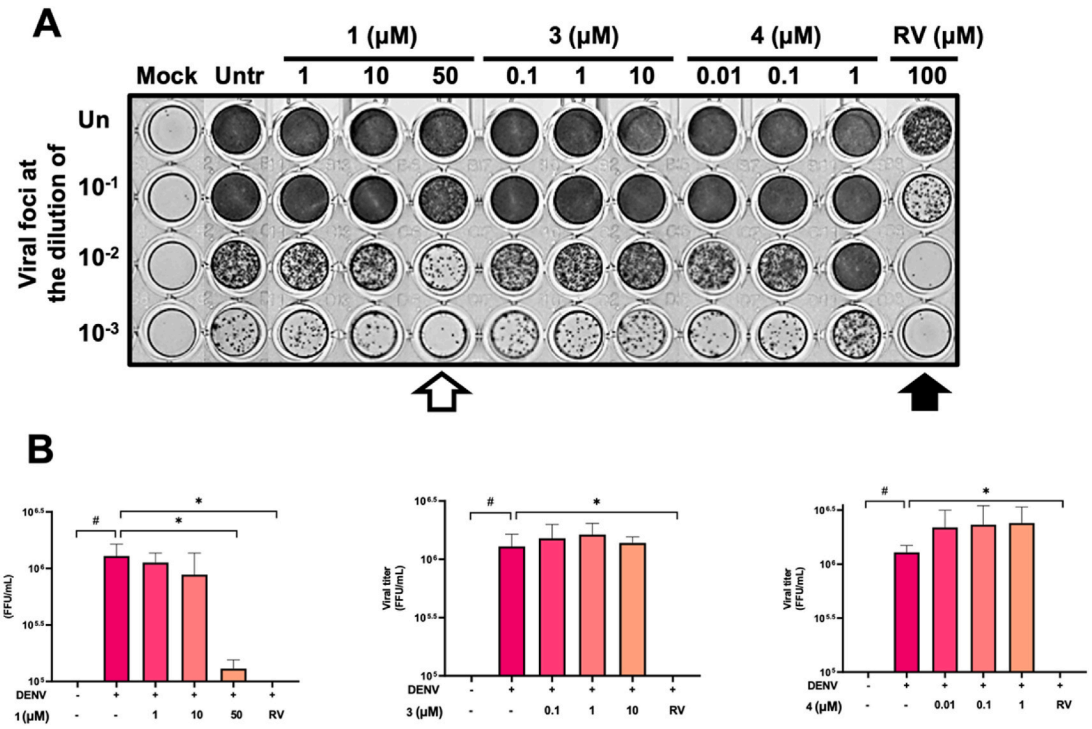

Fig. 6. Compound **1** significantly inhibits DENV infection. DENV-infected Huh7 cells were cultured in the presence or absence of compounds **1** or **3** or **4** at indicated concentrations. Ribavirin (RV) was used as anti-viral positive control. After 24 h, the virus production in the supernatants were quantitated using FFU assay. (A) Representative pictures of virus foci. White and black arrows indicate conditions that reduced viral foci. (B) Bar graph showing viral titers. Data are presented as mean ± SD with three replicates. Statistical significance was determined by one-way ANOVA with Tukey's test; $^{\#}p < 0.05$ vs. mock control, $^{*}p < 0.05$ vs. untreated (Utr).

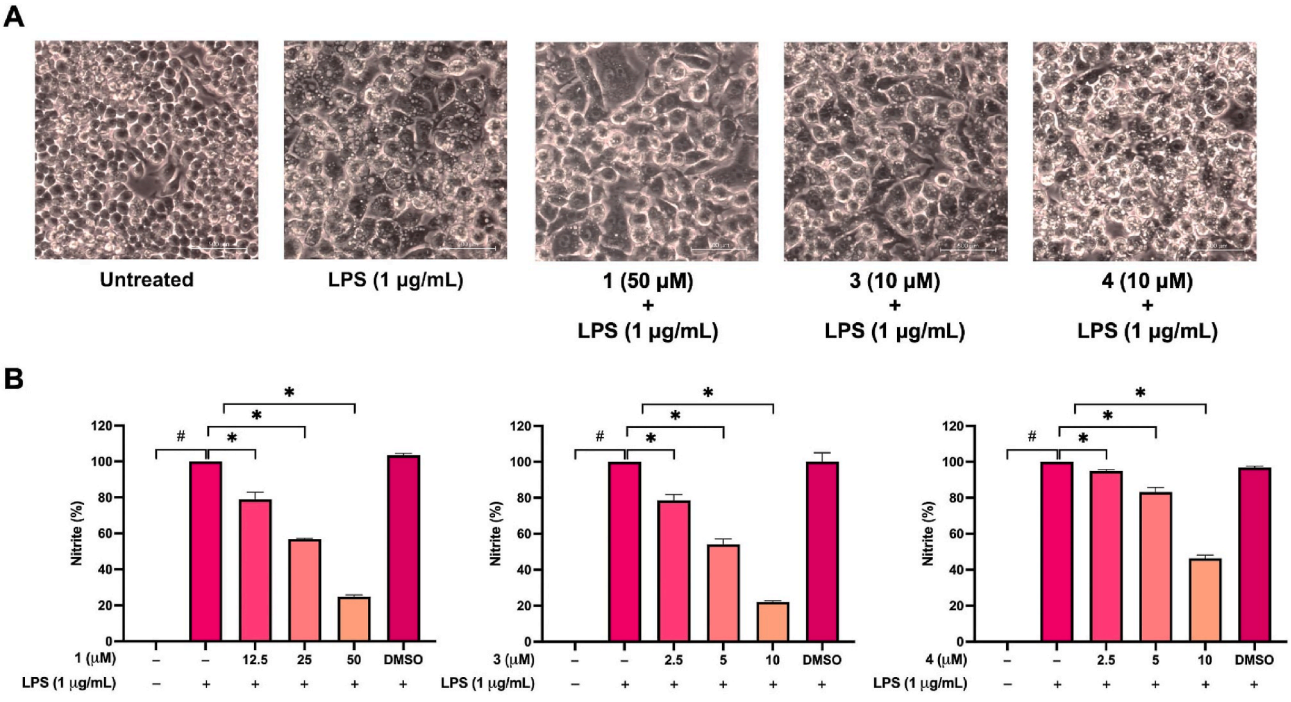

Fig. 7. Compound **3** markedly reduces the production of nitric oxide. RAW264.7 cells were pretreated with various concentrations of compounds **1** or **3** or **4** for 3 h, followed by stimulation with lipopolysaccharide (LPS) for 24 h. Dimethyl sulfoxide (DMSO) was used as negative control. The nitric oxide production in the supernatants was quantified using Griess assay. (A) Representative images of cell morphology that LPS induces irregular, spread-out morphology with pseudopodia, while compounds **1** and **3** treatment preserve a more regular cell shape. The micrographs were captured at 40 × magnification with a scale bar of 500 μm. (B) Bar graph showing nitric oxide production in RAW264.7 cells, expressed as nitrite percentage. Data are presented as mean ± SD with three replicates. Statistical significance was determined by one-way ANOVA with Dunnett's multiple comparisons test; $^{\#}p < 0.05$ vs. untreated control, $^{*}p < 0.05$ vs. LPS alone.

Table 5
Inhibitory effects of compounds on LPS-induced NO production in RAW264.7 cells.

Compounds	IC_{50} (μM)
1	27.85 ± 0.63
3	5.27 ± 0.11
4	9.44 ± 0.14

Data are represented as mean SEM from individual three replicate.

plates at a density of 2×10^5 cells/well and incubated overnight. The cells were then inoculated with dengue virus serotype 2, strain 16681, at a multiplicity of infection (MOI) of 5 for 2 h at 37 °C. After incubation, unbound virus particles were removed by washing with phosphate-buffered saline (PBS). The infected cells were subsequently treated with three non-toxic concentrations of compounds **1**, **3**, and **4** for 24 h. The infected cells treated with 100 μM of ribavirin (RV) served as the positive control. Virus particles secreted into the culture supernatant were quantified using a focus forming unit (FFU) assay in Vero cells. Representative images of viral foci were captured using the ChemiDoc™ Touch Imaging System (Bio-Rad Laboratories). Viral titers were calculated based on the number of foci and expressed as $\log_{10}$ FFU/mL, comparing treated and untreated cells.

4.8. Anti-inflammatory assay

The anti-inflammatory effect of compounds **1**, **3**, and **4** was assessed in RAW264.7 macrophages using Griess assay. RAW264.7 macrophages were cultured and maintained in DMEM medium, supplemented with 10 % FBS and 1 % penicillin-streptomycin-amphotericin-B solution. Then RAW264.7 macrophages were seeded in 24-well plates at a density of 2×10^5 cells/well and incubated overnight. Cells were then pre-treated with three non-toxic concentrations of **1**, **3**, or **4** for 3 h, followed by stimulation with LPS (1 μg/mL) for 24 h. Then morphological changes were examined using a phase-contrast inverted microscope at 40 × magnification, and representative images were captured with a digital camera. Each image includes a 500 μm scale bar. Nitric oxide (NO) production was used to assess anti-inflammatory effect of compounds **1**, **3**, and **4** as previously described (Hankittichai et al., 2020). Briefly, 50 μL of the supernatant from treated RAW264.7 cells was mixed with 50 μL of Griess reagent and incubated at room temperature for 15 min. Absorbance was measured at 540 nm using a TECAN Spark microplate reader, and nitrite concentrations were calculated based on a sodium nitrite standard curve.

CRediT authorship contribution statement

Passakorn Teerapongpisan: Writing – review & editing, Writing – original draft, Investigation, Formal analysis. **Wuttichai Jaidee:** Writing – review & editing, Investigation, Formal analysis. **Theanchai Wiwasuku:** Writing – review & editing, Investigation, Formal analysis. **Sarot Cheenpracha:** Writing – review & editing, Writing – original draft, Formal analysis, Data curation. **Natcha Injan:** Writing – review & editing, Investigation, Formal analysis. **Somkiat Nokbin:** Writing – review & editing, Investigation, Formal analysis. **Kittirat Saharat:** Writing – original draft, Investigation, Formal analysis. **Atthapan Morchang:** Writing – review & editing, Writing – original draft, Investigation, Formal analysis, Data curation. **Phateep Hankittichai:** Writing – original draft, Investigation, Formal analysis, Data curation. **Rawiwan Charoensup:** Writing – review & editing, Resources, Data curation. **Raymond J. Andersen:** Writing – review & editing, Visualization, Supervision, Resources. **Surat Laphookhieo:** Writing – review & editing, Writing – original draft, Visualization, Resources, Project administration, Funding acquisition, Formal analysis, Data curation, Conceptualization.

Declaration of competing interest

On behalf of the authors, I would like to confirm that we have no conflict of interest in the manuscript entitled "Phytochemical study of *Fissistigma fulgens* (Hook.f. & Thomson) Merr. leaves: Previously undescribed dihydrochalcone derivatives and their biological activities" The manuscript is approved by all authors for publication.

Acknowledgements

This work was supported by the National Research Council of Thailand (NRCT) and Mae Fah Luang University (N42A650373). The project was also supported by Reinventing University 2026, which has received funding from the Office of the Permanent Secretary of the Ministry of Higher Education, Science, Research and Innovation, Thailand. We also thank Mr. Abdulromea Baka for plant identification.

Appendix A. Supplementary data

Supplementary data to this article can be found online at https://doi.org/10.1016/j.phytochem.2025.114735.

Data availability

Data will be made available on request.

References

Auranwiwat, C., Rattanajak, R., Kamchonwongpaisan, S., Laphookhieo, S., Pyne, S.G., Limtharakul, T., 2018. Four new *C*-benzyl flavonoids from the fruit of *Uvaria cherrevensis*. Fitoterapia 130, 198–202. https://doi.org/10.1016/j.fitote.2018.08.020.

Chen, I.H., Yang, M.Y., Juang, S.H., Lee, C.L., Thang, T.D., El-Shazly, M., Lan, Y.H., 2018. Bioactive components of *Fissistigma cupreonitens*. Nat. Prod. Commun. 13. https://doi.org/10.1177/1934578X1801300607, 1934578X1801300607.

Chen, J., Jin, C., Xu, B., Shu, J., Shao, F., Yuan, C., Li, F., Huang, L., Huang, H., 2021. New compounds from the stems of *Fissistigma oldhamii* var. longistipitatum and their cytotoxic activities. Fitoterapia 151, 104883. https://doi.org/10.1016/j.fitote.2021.104883.

Dolomanov, O.V., Bourhis, L.J., Gildea, R.J., Howard, J.A., Puschmann, H., 2009. OLEX2: a complete structure solution, refinement and analysis program. J. Appl. Crystallogr. 42, 339–341. https://doi.org/10.1107/S0021889808042726.

Frisch, M.J., Trucks, G.W., Schlegel, H.B., Scuseria, G.E., Robb, M.A., Cheeseman, J.R., Scalmani, G., Barone, V., Petersson, G.A., Nakatsuji, H., Li, X., Caricato, M., Marenich, A., Bloino, J., Janesko, B.G., Gomperts, R., Mennucci, B., Hratchian, H.P., Ortiz, J.V., Izmaylov, A.F., Sonnenberg, J.L., Williams, Y.D., Ding, F., Lipparini, F., Egidi, F., Goings, J., Peng, B., Petrone, A., Henderson, T., Ranasinghe, D., Zakrzewski, V.G., Gao, J., Rega, N., Zheng, G., Liang, W., Hada, M., Ehara, M., Toyota, K., Fukuda, R., Hasegawa, J., Ishida, M., Nakajima, T., Honda, Y., Kitao, O., Nakai, H., Vreven, T., Throssell, K., Montgomery, Jr. J.A., Peralta, J.E., Ogliaro, F., Bearpark, M., Heyd, J.J., Brothers, E., Kudin, K.N., Staroverov, V.N., Keith, T., Kobayashi, R., Normand, J., Raghavachari, K., Rendell, A., Burant, J.C., Iyengar, S.S., Tomasi, J., Cossi, M., Millam, J.M., Klene, M., Adamo, C., Cammi, R., Ochterski, J.W., Martin, R.L., Morokuma, K., Farkas, O., Foresman, J.B., Fox, D.J., 2009. Gaussian 09 (Revision A.02). Gaussian, Inc., Wallingford, CT.

Hadi, A.H.A., 2000. Alkaloids from *Fissistigma fulgens* merr. Annonaceae. Malays. J. Sci. 19, 41–44.

Hankittichai, P., Buacheen, P., Pitchakarn, P., Na Takuathung, M., Wikan, N., Smith, D.R., Potikanond, S., Nimlamool, W., 2020. *Artocarpus lakoocha* extract inhibits LPS-induced inflammatory response in RAW 264.7 macrophage cells. Int. J. Mol. Sci. 21, 1355. https://doi.org/10.3390/ijms21041355.

Jaidee, W., Andersen, R.J., Chavez, M.A., Wang, Y.A., Patrick, B.O., Pyne, S.G., Muanprasat, C., Borwornpinyo, S., Laphookhieo, S., 2019. Amides and flavonoids from the fruit and leaf extracts of *Melodorum siamensis*. J. Nat. Prod. 82, 283–292. https://doi.org/10.1021/acs.jnatprod.8b00696.

Jin, C., Zhang, L., Yuan, C.J., Liu, Y., Liu, H.Z., Xu, B.L., Shu, J.C., Zhang, X.Y., Wang, S.Y., Huang, H.L., 2023. New compounds from the stems of *Fissistigma acuminatissimum* Merr. and their *in vitro* anti-inflammatory activity. Nat. Prod. Res. 37, 551–559. https://doi.org/10.1080/14786419.2022.2076231.

Kang, J., Xie, C., Li, Z., Nagarajan, S., Schauss, A.G., Wu, T., Wu, X., 2011. Flavonoids from acai (*Euterpe oleracea* Mart.) pulp and their antioxidant and anti-inflammatory activities. Food Chem. 128, 152–157. https://doi.org/10.1016/j.foodchem.2011.03.011.

Koudokpon, H., Armstrong, N., Dougnon, T.V., Fah, L., Hounsa, E., Bankolé, H.S., Loko, F., Chabrière, E., Rolain, J.M., 2018. Antibacterial activity of chalcone and dihydrochalcone compounds from *Uvaria chamae* roots against multidrug-resistant bacteria. BioMed Res. Int. 2018, 1453173. https://doi.org/10.1155/2018/1453173.

Kurkina, A.V., Ryazanova, T.K., Kurkin, V.A., 2013. Flavonoids from the aerial part of *Polygonum hydropiper*. Chem. Nat. Compd. 49, 830–832. https://doi.org/10.1007/s10600-013-0758-y.

Lam, P.Y., Lui, A.C., Wang, L., Liu, H., Umezawa, T., Tobimatsu, Y., Lo, C., 2021. Tricin biosynthesis and bioengineering. Front. Plant Sci. 12, 733198. https://doi.org/10.3389/fpls.2021.733198.

Lan, Y.H., Chia, Y.C., Chang, F.R., Hwang, T.L., Liaw, C.C., Wu, Y.C., 2005. Potential anti-inflammatory activities of Bractelactone and other compounds isolated from *Fissistigma bracteolatum*. Helv. Chim. Acta 88, 905–909. https://doi.org/10.1002/hlca.200590068.

Lan, Y.H., Leu, Y.L., Peng, Y.T., Thang, T.D., Lin, C.C., Bao, B.Y., 2011. The first bis-retrochalcone from *Fissistigma latifolium*. Planta Med. 77, 2019–2022. https://doi.org/10.1055/s-0031-1280088.

Low, J.G., Ooi, E.E., Vasudevan, S.G., 2017. Current status of dengue therapeutics research and development. J. Infect. Dis. 215, S96–S102. https://doi.org/10.1093/infdis/jiw423.

Morchang, A., Malakar, S., Poonudom, K., Noisakran, S., Yenchitsomanus, P.T., Limjindaporn, T., 2021. Melatonin inhibits dengue virus infection via the sirtuin 1-mediated interferon pathway. Viruses 13, 659. https://doi.org/10.3390/v13040659.

Ngoc, H.N., Mair, L., Nghiem, D.T., Le Thien, K., Gostner, J.M., Stuppner, H., Ganzera, M., 2019. Phenolic compounds from the stems of *Fissistigma polyanthoides* and their anti-oxidant activities. Fitoterapia 137, 104252. https://doi.org/10.1016/j.fitote.2019.104252.

Pi, J., Li, T., Liu, J., Su, X., Wang, R., Yang, F., Bai, H., Jin, H., Cai, J., 2014. Detection of lipopolysaccharide induced inflammatory responses in RAW264. 7 macrophages using atomic force microscope. Micron 65, 1–9. https://doi.org/10.1016/j.micron.2014.03.012.

Saharat, K., Paramee, N., Parichartanakul, N.M., Rangkadilok, N., Chokchaichamnankit, D., Srisomsap, C., Lirdprapamongkol, K., Svasti, J., Satayavivad, J., 2025. Unveiling the benefit of germinated colored rice extract to decrease metastatic potential of colorectal cancer cells. J. Funct.Foods 124, 106655. https://doi.org/10.1016/j.jff.2024.106655.

Salae, A.W., Chairerk, O., Sukkoet, P., Chairat, T., Prawat, U., Tuntiwachwuttikul, P., Chalermglin, P., Ruchirawat, S., 2017. Antiplasmodial dimeric chalcone derivatives from the roots of *Uvaria siamensis*. Phytochemistry 135, 135–143. https://doi.org/10.1016/j.phytochem.2016.12.009.

Saxena, R.K., Vallyathan, V., Lewis, D.M., 2003. Evidence for lipopolysaccharideinduced differentiation of RAW264. 7 murine macrophage cell line into dendritic like cells. J. Bio. Sci. 28, 129–134. https://doi.org/10.1007/BF02970143.

Sheldrick, G.M., 2015a. SHELXT-Integrated space-group and crystal-structure determination. Acta Crystallogr. A71, 3–8. https://doi.org/10.1107/S2053273314026370.

Sheldrick, G.M., 2015b. Crystal structure refinement with SHELXL. Acta Crystallogr. C71, 3–8. https://doi.org/10.1107/S2053229614024218.

Sudha, A., Srinivasan, P., 2014. Bioassay-guided isolation and antioxidant evaluation of flavonoid compound from aerial parts of *Lippia nodiflora* L. BioMed Res. Int. 2014, 549836. https://doi.org/10.1155/2014/549836.

Wirasathien, L., Pengsuparp, T., Moriyasu, M., Kawanishi, K., Suttisri, R., 2006. Cytotoxic *C*-benzylated chalcone and other constituents of *Ellipeiopsis cherrevensis*. Arch Pharm. Res. (Seoul) 29, 497–502. https://doi.org/10.1007/BF02969423.